AGU PUBLICATIONS

JGR

Journal of Geophysical Research: Space Physics

RESEARCH ARTICLE
10.1002/2016JA023846

Key Points:
- Radial diffusion coefficient calculated from LFM MHD model agrees with the diffusion coefficient calculated from RBSP measurements
- Radial diffusion coefficient calculated from LFM MHD model is much lower than Bratigam and Albert and Ozeke's
- Agreement between radial diffusion model and RBSP measurement was much improved using radial diffusion coefficients from the MHD simulations

Correspondence to:
Z. Li,
zhao.li@dartmouth.edu

Citation:
Li, Z., M. Hudson, M. Patel, M. Wiltberger, A. Boyd, and D. Turner (2017), ULF wave analysis and radial diffusion calculation using a global MHD model for the 17 March 2013 and 2015 storms, *J. Geophys. Res. Space Physics*, *122*, 7353–7363, doi:10.1002/2016JA023846.

Received 27 DEC 2016
Accepted 23 MAY 2017
Accepted article online 1 JUN 2017
Published online 17 JUL 2017

ULF wave analysis and radial diffusion calculation using a global MHD model for the 17 March 2013 and 2015 storms

Zhao Li[1], Mary Hudson[1], Maulik Patel[1], Michael Wiltberger[2], Alex Boyd[3], and Drew Turner[4]

[1]Department of Physics and Astronomy, Dartmouth College, Hanover, New Hampshire, USA, [2]High Altitude Observatory, National Center for Atmospheric Research, Boulder, Colorado, USA, [3]New Mexico Consortium, Los Alamos, New Mexico, USA, [4]Aerospace Corporation, El Segundo, California, USA

Abstract The 17 March 2015 St. Patrick's Day Storm is the largest geomagnetic storm to date of Solar Cycle 24, with a *Dst* of −223 nT. The magnetopause moved inside geosynchronous orbit under high solar wind dynamic pressure and strong southward interplanetary magnetic field B_z causing loss; however, a subsequent drop in pressure allowed for rapid rebuilding of the radiation belts. The 17 March 2013 storm also shows similar effects on outer zone electrons: first, a rapid dropout due to inward motion of the magnetopause followed by rapid increase in flux above the prestorm level early in the recovery phase and a slow increase over the next 12 days. These phases can be seen in temporal evolution of the electron phase space density measured by the Energetic Particle, Composition, and Thermal Plasma Suite (ECT) instruments on Van Allen Probes. Using the Lyon-Fedder-Mobarry global MHD model driven by upstream solar wind measurements, we simulated both St. Patrick's Day 2013 and 2015 events, analyzing Lyon-Fedder-Mobarry electric and magnetic fields to calculate radial diffusion coefficients. These coefficients have been implemented in a radial diffusion code, using the measured electron phase space density following the local heating as the initial radial profile and outer boundary condition for subsequent temporal evolution over the next 12 days, beginning 18 March. Agreement with electron phase space density at 1000 MeV/G measured by the MagEIS component of the ECT instrument suite on Van Allen Probes was much improved using radial diffusion coefficients from the MHD simulations relative to coefficients parameterized by a global geomagnetic activity index.

1. Introduction

The Earth's outer radiation belt, which consists of relativistic electrons trapped in the Earth's magnetic field, is known to be highly dynamic in response to variations in solar wind driving conditions. These include interplanetary shocks driven by Coronal Mass Ejections (CMEs) which are dominant drivers at solar maximum and Corotating Interaction Regions (CIRs) mapping to coronal holes which are dominant drivers during the declining phase of the solar cycle [*Tsurutani and Gonzalez*, 1997; *Tsurutani et al.*, 2006; *Hudson et al.*, 2008, 2012]. These MeV electrons pose a significant space weather hazard to spacecraft and astronauts. Understanding the evolution of the Earth's relativistic electron population is a primary goal of NASA's Van Allen Probes mission, twin satellites launched on 30 August 2012, during the recent weak solar maximum [*Mauk et al.*, 2013]

The 17 March 2015 St. Patrick's Day Storm is the largest geomagnetic storm to date of Solar Cycle 24, with a *Dst* of −223 nT. The magnetopause moved inside geosynchronous orbit under high solar wind dynamic pressure and strong IMF B_z causing loss; however, a subsequent drop in pressure allowed for rapid rebuilding of the radiation belts [*Kanekal et al.*, 2016]. Local heating has been modeled for this and the 17 March 2013 storm [*W. Li et al.*, 2014], weaker at *Dst* of −132 nT and showing similar MeV electron flux changes: first, a rapid dropout due to inward motion of the magnetopause followed by rapid increase in flux above the prestorm level during the recovery phase. These phases can be seen in temporal evolution of the electron phase space density measured by the ECT instruments on Van Allen Probes [*Spence et al.*, 2014].

Prompt loss of electrons due to inward motion of the magnetopause following a CME shock arrival and subsequent outward diffusive radial transport has been shown to characterize the initial phase of CME shock-initiated storms [*Shprits et al.*, 2006; *Hudson et al.*, 2014, 2015]. Both local heating and radial transport

result in an increase in flux at a fixed energy and constitute competing mechanisms which have been suggested to explain the enhancement phase [*Shprits et al.*, 2008a, 2008b; *Thorne*, 2010]. (ULF) waves are important in transporting radiation belt electrons, because their frequency is in the mHz range, comparable to the relativistic electron drift frequency in the outer zone [*Elkington et al.*, 2003; *Perry et al.*, 2005; *Shprits et al.*, 2008a]. If an electron experiences an approximately constant azimuthal electric field in its drift frame, it can be accelerated or decelerated by the wave field. Conserving its first two adiabatic invariants, the electron will be transported inward or outward depending on the sign of electric field antiparallel or parallel to its drift motion. Such interaction can be coherent or a stochastic random walk process depending on the spectral coherence of the ULF waves [*Elkington et al.*, 2003]. Changes in the convection electric field also cause both coherent and diffusive radial transport. Many models have incorporated the effects of changing convection electric field into modeling such transport of plasma sheet electrons and ions into the inner magnetosphere, see, for example, *Jordanova et al.* [2014], *Fok et al.* [2014], *Kress et al.* [2014], and *Gabrielse et al.* [2016], along with radial diffusion models going back to *Fälthammar* [1965].

Global MHD simulations driven by upstream solar wind parameters specify fields for both types of radial transport: those due to ULF waves and to variations in the convection electric field. The mechanisms for exciting ULF waves in the mHz frequency range have been investigated using MHD simulations [*Claudepierre et al.*, 2016] dividing excitation mechanisms into Kelvin-Helmoholz instability due to velocity shear along the magnetopause [*Claudepierre et al.*, 2008] and transfer of ULF oscillations in the solar wind into the magnetosphere [*Claudepierre et al.*, 2010] for idealized simulations. MHD simulations do not capture the high *m* number poloidal modes excited by drift bounce resonance [*Southwood and Kivelson*, 1981] which have little resonant effect on MeV radiation belt electrons [*Ozeke and Mann*, 2004].

Recent statistical studies of measured magnetic and electric field wave power in the mHz frequency range, both on the ground [*Ozeke et al.*, 2014] and in space [*Ali et al.*, 2016], have been parameterized by the global geomagnetic activity index *Kp* and used to compute radial transport coefficients. This paper will compare with those studies for specific event simulations analyzing electric and magnetic fields in the mHz frequency range calculated using the Lyon-Fedder-Mobarry MHD code [*Lyon et al.*, 2004]. Upstream solar wind parameters are taken from OMNIWeb for the March 2013 storm and the ARTEMIS spacecraft [*Angelopoulos*, 2009] for the March 2015 storm, used previously as input to simulation of the 7–8 October 2013 storm [*Hudson et al.*, 2015]. The ARTEMIS measurements have higher time resolution (6 s) when available than the OMNIWeb solar wind measurements from ACE and Wind (1 min) used for other storms [*Hudson et al.*, 2015]. Magnetosphere-ionosphere coupling is handled in our simulations of the 17–18 March 2013 and 2015 storms using the Magnetosphere-Ionosphere-Coupler (MIX) code [*Merkin and Lyon*, 2010], which also handles coupling to the Rice Convection Model (RCM) [*Pembroke et al.*, 2012] used in the present study for comparison of the simulated background magnetic field with measurements for both storms.

2. Calculation of Radial Diffusion Coefficients

Both the 17 March 2013 and 2015 storms produced strong enhancements of outer zone electrons with the 2015 storm producing the strongest enhancement of the ring current seen in Solar Cycle 24 in terms of *SYM-H* (a symmetric disturbance index describing the horizontal geomagnetic disturbance fields, similar to *Dst* index) [*Baker et al.*, 2014; *Kanekal et al.*, 2016]. Solar wind speed, IMF *By*, IMF *Bz*, and *SYM-H* are plotted in Figures 1 (top) and 1 (bottom) for both storms. A strong CME shock hit the Earth's magnetosphere at 0604 UT in Figure 1 (top) and at 0445 UT in Figure 1 (bottom). The magnetopause moved inside geosynchronous orbit under high solar wind dynamic pressure and strong southward IMF *Bz* for the 2015 storm [*Le et al.*, 2016], while it was strongly compressed close to geosynchronous orbit for the 2013 storm [*Hudson et al.*, 2015].

The Lyon-Fedder-Mobarry (LFM) global MHD model implemented with the Magnetosphere-Ionosphere-Coupler (MIX) is run for 17–18 March 2013 and 2015 at a grid resolution of $106 \times 96 \times 128$ in radial, azimuthal, and polar directions. Results with and without RCM coupling are plotted in the bottom panels of Figures 1 (top) and 1 (bottom) showing simulated *SYM-H* calculated from a Biot-Savart integration compared with measured *SYM-H*. To further evaluate LFM performance, we compare the magnitude of the magnetic field at simulated GOES locations from LFM with GOES 13 and 15 satellite measurements of magnetic field, shown in Figure 2

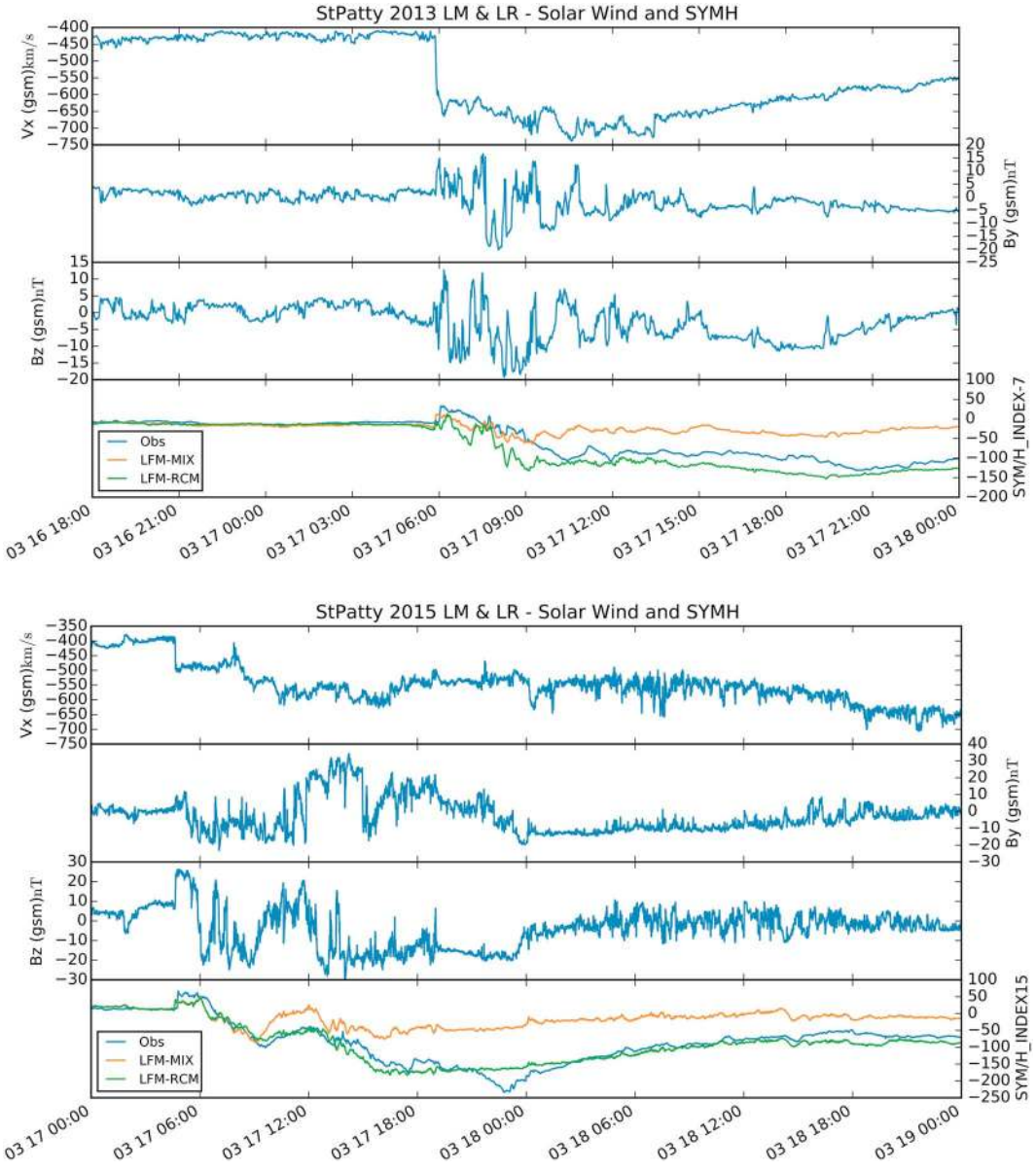

Figure 1. Solar wind speed, IMF B_y, IMF B_z, and *SYM-H* on (top) 17–18 March 2013 and (bottom) 17–18 March 2015.

for the March 2013 storm [*Li et al.*, 2015]. For the ULF wave analysis presented next, we use fields from the LFM-MIX simulations of 17–18 March 2013 and 2015. ULF wave analysis has been repeated for the fields obtained from the LFM-RCM simulations with little change from the results presented here after 1200 UT on the second day of each storm. This result indicates that the effects of RCM coupling are greater for the background DC field than at ULF wave frequencies. Radial diffusion analysis will be restricted to the recovery phase of both storms when local heating can be incorporated as an initial condition in the measured phase space density profile and diffusion coefficients from LFM-RCM and LFM-MIX converge.

At each time step, the fluctuating electric field is decomposed into the symmetric and asymmetric components for successive radial distances [*Elkington et al.*, 2012]. Then, at each radial location, the DC component is removed by subtracting the mean value of a 30 min signal centered at each time step. The data are then multiplied by a Hanning window and processed by Fast Fourier transform [*Li et al.*, 2016]. The reverse order aliases DC power to low frequencies due to windowing of the DC component. *Fei et al.* [2006] derived the

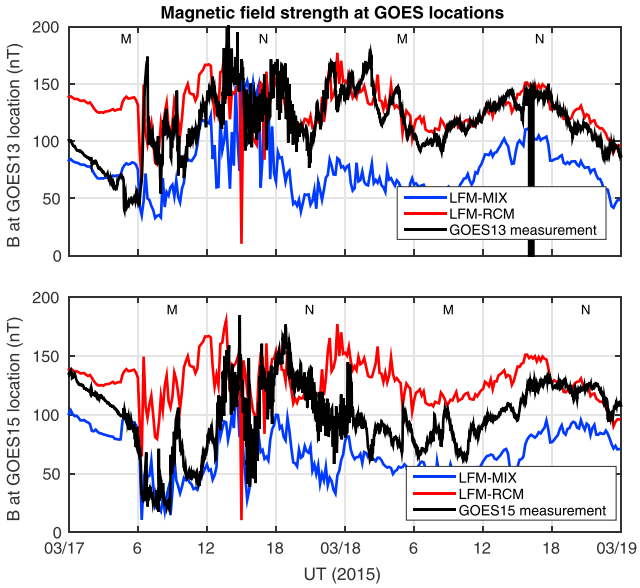

Figure 2. LFM-MIX (blue), LFM-RCM (red), and measured (black) magnetic field strength at GOES 13 and GOES 15 locations for the March 2015 storm [*Li et al.*, 2016].

radial diffusion coefficients in a dipole magnetic field as a function of ULF wave power following *Brizard and Chan* [2001], separated into electric and magnetic field contributions:

$$D_{LL}^{E} = \frac{1}{8\,B_E^2 R_E^2} L^6 \sum_m P_m^E(m\omega_d) \tag{1a}$$

$$D_{LL}^{B} = \frac{M^2}{8q^2\gamma^2 B_E^2 R_E^4} L^4 \sum_m m^2 P_m^B(m\omega_d) \tag{1b}$$

In our calculation, we include the power of all azimuthal mode numbers where $m\omega_d$ is lower than the Nyquist frequency 8.3 mHz, m is the azimuthal mode number, and ω_d is the azimuthal drift frequency. *Li et al.* [2016] have plotted the fluctuating electric and magnetic field power spectrum as a function of L, radial distance in the solar magnetic (SM) equatorial plane in Earth radii, and m. The power along straight lines which satisfy the drift resonant condition for a given first invariant, $\omega = m\omega_d$, is inserted into equations (1a) and (1b)

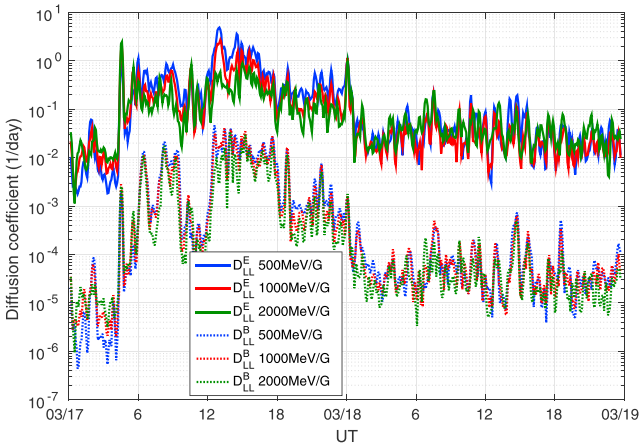

Figure 3. Electric (solid lines) and magnetic (dashed lines) radial diffusion coefficient at geosynchronous for three first invariants: 500 MeV/G (blue), 1000 MeV/G (red), and 2000 MeV/G (green), integrated over mode numbers at corresponding drift resonant frequencies from 0.5–8.3 mHz [*Li et al.*, 2016].

to calculate the diffusion coefficient at each L value due to electric and magnetic field fluctuations, and plotted in Figure 3 at geosynchronous orbit for three values of the first invariant for the March 2015 storm. D_{LL}^{E} and D_{LL}^{B} both increase for all first invariants as geomagnetic activity level increases and the dependence on the first invariant is very weak for both D_{LL}^{E} and D_{LL}^{B}. Computed D_{LL}^{E} dominates D_{LL}^{B}, which is consistent with the *Ali et al.* [2016] result using electric and magnetic field measurements from Van Allen Probes over 3 years. A recent study by *Ozeke et al.* [2014] shows similar dominance of D_{LL}^{E}, inferring equatorial plane azimuthal electric field from ground magnetometer measurements assuming a standing Alfven wave model. Both statistical models also confirm lack of dependence on first invariant and therefore energy. Comparisons with other models for D_{LL} are deferred to section 5.

3. Solution of Radial Diffusion Equation

Relativistic electrons trapped in the Earth's magnetic field undergo three types of periodic motion: gyromotion around the field lines, bounce motion along field lines, and drift motion around the Earth. Three invariants are related to the three types of periodic motion: gyro, bounce, and drift. The three adiabatic invariants and their phase angle form a set of canonical variables. By averaging over three phase angles, setting the second invariant to zero for equatorially mirroring electrons, and representing violation of the first invariant M, or magnetic flux through the gyro orbit, by a loss term, the Fokker-Planck equation reduces to

$$\frac{\partial}{\partial t} f(M, L^*) = L^{*2} \frac{\partial}{\partial L^*} \left(D_{LL} L^{*2} \frac{\partial f}{\partial L^*} \right) - \frac{f}{\tau} \tag{2}$$

Here L^* defined by *Roederer* [1970] is inversely proportional to the magnetic flux through a drift orbit and requires a magnetic field model specification. We use TS04 to solve the radial diffusion equation in L^* incorporating effects of adiabatic changes such as the buildup and relaxation of the ring current, the so-called *Dst* effect [*Kim and Chan*, 1997]. The International Radiation Belt Environment Modeling (IRBEM) library (https://craterre.onecert.fr/prbem/irbem/description.html) is used to transform D_{LL} calculated in L from LFM into L^* for implementation in the radial diffusion calculation. The second term on the right-hand side of equation (2) represents *Kp* parameterized pitch angle scattering loss to the atmosphere. We implement a different loss model inside and outside of the plasmapause to model hiss [*Orlova and Shprits*, 2014] and chorus [*Orlova et al.*, 2014] loss, respectively. We have used both a *Kp* parameterized plasmapause in our radial diffusion model [*Carpenter and Anderson*, 1992; *Li et al.*, 2014a] and a plasmapause location determined from measuring spacecraft potential with the Electric Fields and Waves (EFW) instrument on Van Allen Probes [*Wygant et al.*, 2014; *Li et al.*, 2014b] with little difference in radial diffusion results for the two plasmapause models during the recovery phase modeled here, beginning 0000 UT 18 March 2013 and 2015.

To investigate the role of radial diffusion and test the diffusion coefficients obtained from MHD simulations, it is necessary to implement boundary conditions. Figure 4 shows 1000 MeV/G electron phase space density (PSD) from successive orbits calculated using Van Allen Probes (RBSP-A) measurements from the medium energy (30 keV to 4 MeV) MagEIS instrument from the ECT suite [*Blake et al.*, 2013] for the March 2015 storm. The measurements show an initial increase in PSD with L^*, which is inversely proportional to magnetic flux inside a drift orbit [*Roederer*, 1970], calculated using the TS04 magnetic field model. Evidence for local heating is seen for the orbit beginning 0000 UT on 18 March, when a peak at $L^* \sim 4$ is measured. On subsequent orbits, continued inward radial transport of electrons from their plasma sheet source appears evident while local heating around $L^* \sim 4$ may continue to enhance outward radial transport [*Reeves et al.*, 2013]. The compression of the magnetosphere is evident as the radial profile extending to Van Allen Probes apogee initially moves inward over sequential orbits and then relaxes radially in L^*. This relaxation of the L to L^* mapping continues over subsequent days.

In order to incorporate the effects of local heating, the model uses the MagEIS radial profile for 1000 MeV/G at 0000 UT on 18 March 2013 (2015) and the corresponding MagEIS flux measurements at apogee converted to phase space density f as the outer boundary condition, along with the assumption that f vanishes at the inner boundary. The European Space Agency (ESA) statistical model based on measurements from the Combined Release and Radiation Effects Satellite [*Vampola*, 1996] is adjusted to the MagEIS observation at $L^* = 4.3$ for the grid points outside the Van Allen Probes apogee. The outer boundary adjusts to the L^* value of f measurements over the 12 day radial diffusion calculation. The average diffusion coefficient, which is relatively constant on 18 March in Figure 3, and the corresponding plot for 2013, is used over the next 12 days,

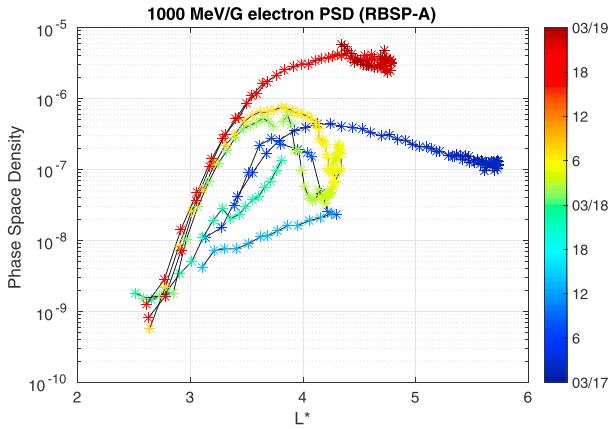

Figure 4. The 1000 MeV/G electron phase space density calculated using RBSP-A MagEIS measurement for 17–18 March 2015.

while dynamically mapping from L (radial distance in the SM equatorial plane of the MHD simulation) to L^* using TS04 as the magnetosphere relaxes poststorm. This dynamic mapping is also implemented in the outer boundary condition on f determined from the Van Allen Probes apogee measurement. At the beginning of 18 March the radial profile has a peak around L^*=3.5–4 in Figure 5a (4–5 in Figure 5c). This peak relaxes as a result of outward diffusion along with inward radial transport from the outer boundary as measured by the flux and f update at the apogee of Van Allen Probes mapped into L^*. The relaxation of this outer boundary is indicated by the two horizontal black lines showing the initial (bottom) and final (top) apogee over the 12 day simulation.

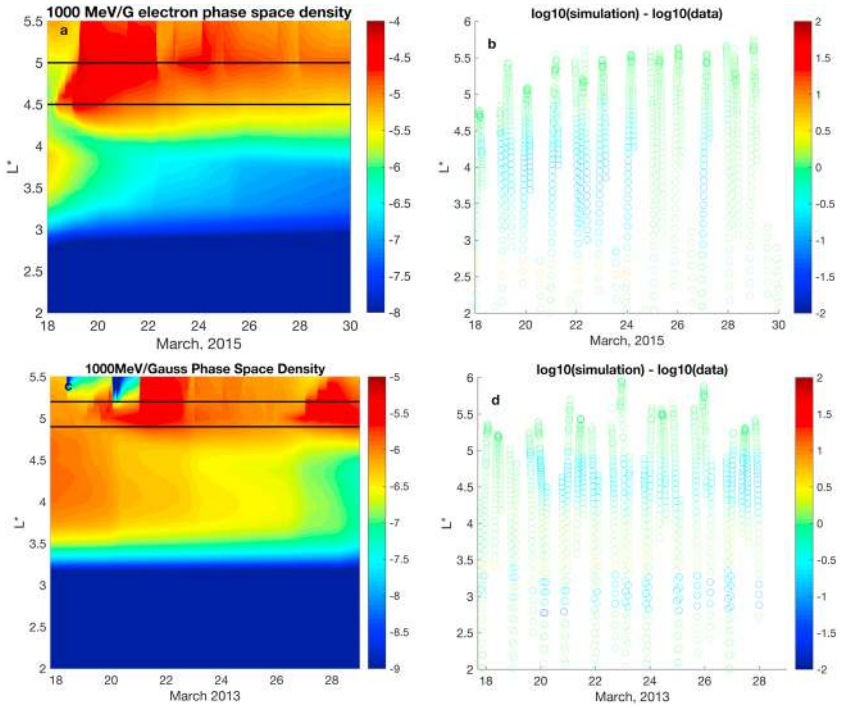

Figure 5. (a) The 1000 MeV/G electron phase space density calculated using radial diffusion model for the March 2015 storm. (b) Error between simulation and MagEIS measurement. (c) Same as Figure 5a but for March 2013 storm. (d) Same as Figure 5b for March 2013 storm. Black lines indicate range of Van Allen Probes apogee from 00 UT on 18 March (bottom line) near *SYM-H* minimum to end of event study (top line) when magnetosphere has relaxed. The simulation domain outside the MagEIS outer boundary is the "ghost cell," as discussed in *Li et al.* [2014a], and should be ignored as it is likely that flux continues to increase at higher L^* but is set to $f = 0$ at $L^* = 10$. Note that 1000 MeV/G measurements are at background levels inside $L^* \sim 2.75$.

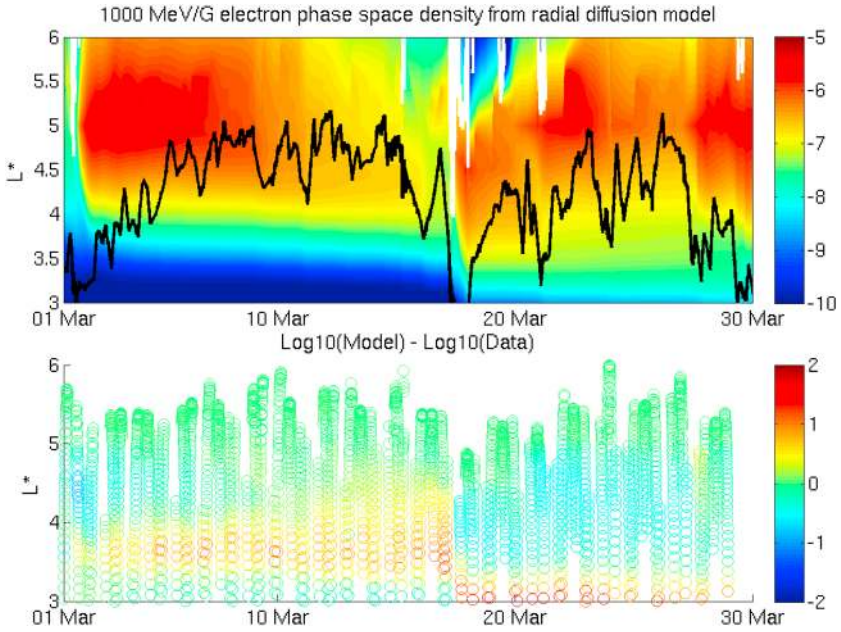

Figure 6. (top) Electron phase space density calculated using radial diffusion model for $M = 1000$ MeV/G, $K = 0.0100R_E G^{1/2}$. The black line is the plasmapause location measured by the EFW instrument, converted to L^* using T96 magnetic field model, close to TS05 at low L^*. The white line shows the last closed drift shell, outside the plotting domain most of the time. (bottom) Error between the radial diffusion model and Van Allen Probes MagEIS data [*Li et al.*, 2014a].

4. Comparison With Van Allen Probes MagEIS Measurements

To compare with the Van Allen Probes MagEIS measurements, the error Log10(Model) − Log10(Data) is plotted in Figures 5b and 5d for both storms. This subtraction between the radial diffusion model for phase space density and that measured yields an error less than 0.5 orders of magnitude (3.2 times). These results are significantly improved over what is obtained using a radial diffusion coefficient in wide use developed by *Brautigam and Albert* [2000], based on a limited set of ground and geosynchronous satellite measurements. *Li et al.* [2014a] performed analysis similar to that shown in Figure 5 for the entire month of March 2013, reproduced in Figure 6, using the *Kp* parameterized *Brautigam and Albert* [2000] D_{LL} coefficients and the same outer boundary condition used in Figure 5. A careful analysis was given by *Ali et al.* [2016] of the distinction between *Brautigam and Albert* [2000] D_{LL} coefficients, neglecting an electrostatic contribution shown to be minor, but including the induction electric field as well as magnetic contribution implied by Faraday's Law, contained in the radial diffusion coefficients of equation (2). The radial diffusion code using *Brautigam and Albert* [2000] diffusion coefficients overestimates phase space density at $L^* = 3.5–4$ in the first half of the month of March 2013 following a CIR-driven storm [*Baker et al.*, 2014] and underestimates *f* by more than an order of magnitude during the recovery phase of the CME shock-driven storm beginning 18 March 2013, when compared with Figure 5. We conclude that implementation of diffusion coefficients based on the MHD event studies and incorporation of measured boundary conditions from Van Allen Probes (initial radial profile and outer boundary) significantly improve the comparison with MagEIS measurements at 1000 MeV/G over the 12 days following minimum *SYM-H* for the March 2013 storm. A caveat in all radial diffusion calculations compared with measured flux converted to phase space density profiles is the competition between source and loss processes. Our model isolates those due to radial transport and modeled loss to the atmosphere.

5. Discussion and Conclusions

Determination of radial diffusion coefficients based on in situ measurements, as recently carried out by *Ali et al.* [2016] using Van Allen Probes electric and magnetic field data, and studies incorporating ground-based measurements like *Ozeke et al.* [2014] using the CARISMA magnetometer chain, supplemented by in situ measurements of compressional *B*, requires a statistical parameterization by geomagnetic activity level. *Kp* has typically been used, following the parameterization of D_{LL} by *Brautigam and Albert* [2000] who used

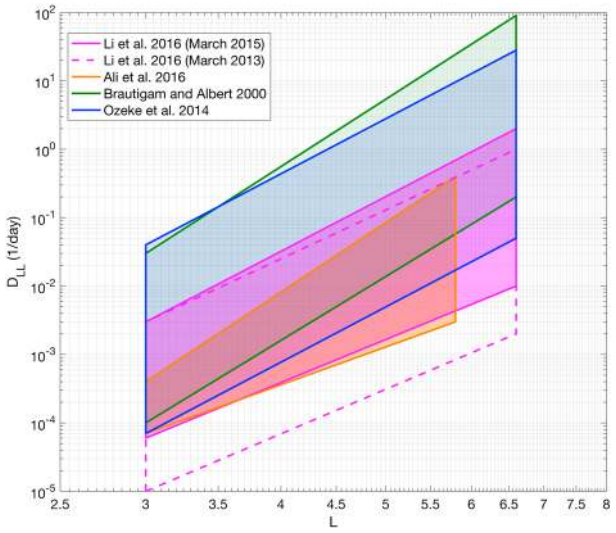

Figure 7. Comparisons of radial diffusion coefficients D_{LL} from LFM-MIX simulations of the March 2013 and 2015 storms (dashed and solid purple) with those from *Ali et al.* [2016] (yellow), *Ozeke et al.* [2014] (blue), and *Brautigam and Albert* [2000] (green).

geosynchronous magnetometer measurements and ground-based magnetometer measurements at $L = 4.2$ to sort magnetic perturbations by *Kp* [*Lanzerotti and Morgan*, 1973; *Lanzerotti et al.*, 1978] over a limited time span of 6 months. Models parameterized by *Kp* are plotted as trapezoids in Figure 7, green corresponding to *Brautigam and Albert* [2000], blue to *Ozeke et al.* [2014], and yellow to *Ali et al.* [2016]. These comparisons are fraught with the need to compare the total diffusion coefficient as has been done in Figure 7, where both electric and magnetic field contributions have been included, in contrast to comparisons of partial contributions as, for example, *Liu et al.* [2016] have done solely with THEMIS electric field measurements. *Brautigam and Albert* [2000] coefficients are based on a calculation by *Fälthammar* [1968] which assumes a magnetic fluctuation spectrum which varies inversely with frequency and has a resulting L^{10} dependence, implicitly including inductive electric field fluctuations. A companion electrostatic D_{LL} calculation based on *Fälthammar* [1965] and *Cornwall* [1968] was shown in their paper to be negligible.

We have used the same separation of field power into electric and magnetic as given in equations (1a) and (1b) and originally used by *Fei et al.* [2006] who first calculated diffusion coefficients from an earlier version of the stand-alone LFM global MHD simulation for specified solar wind input corresponding to the 24 September 1998 CME shock-driven storm. We focus on the ULF wave contribution in which the electric field is inductive and have found, as have *Ozeke et al.* [2014] and *Ali et al.* [2016] in their implementations of equations (1a) and (1b), that the electric field component is dominant. Other studies using LFM driven by parameterized solar wind velocity and measured upstream input parameters were performed by *Huang et al.* [2010] and *Tu et al.* [2012], respectively, under assumptions which produce results bracketing those presented here [*Li et al.*, 2016, Figure 8]. Our results bound those obtained by *Ali et al.* [2016], which were limited to time intervals with *Kp* at or below 5, due to the moderate activity level since the launch of Van Allen Probes in 2012. We have focused on two storms where *Kp* exceeded that used in the statistical studies, with maximum $Kp = 6.7$ on 17 March 2013 and $Kp = 7.7$ on 17 March 2015.

What can we conclude about the larger D_{LL} values obtained by *Brautigam and Albert* [2000] and *Ozeke et al.* [2014]? Both yield larger *Kp*-parameterized diffusion coefficients than *Ali et al.* [2016]. Neither uses direct measurement of electric fields in situ as *Ali et al.* [2016] has included and we have incorporated from analysis of MHD fields. There are certainly caveats in the use of the *Brizard and Chan* [2001] formulation, now in prevalent use when it is not possible or straightforward to separate an electrostatic from an inductive electric field contribution. They are based on the assumption of random correlation between electric and magnetic field perturbations about a background dipole magnetic field. The ULF waves analyzed in our simulations, and the statistical measurement-based studies of *Ozeke et al.* [2014] and *Ali et al.* [2016], do not satisfy these assumptions in a strict sense. However, fewer assumptions are made than, for example, the $D_{LL} \sim L^{10}$ assumption by *Brautigam and Albert* [2000], which is not born out even in the two-point fit to $L = 4$ and $L = 6.6$

measurements in Figure 5 of their paper, where it can be seen that D_{LL} has a stronger (weaker) dependence on L with lower (higher) Kp than L^{10}. Similarly, *Ozeke et al.* [2014] assume a standing Alfven wave model to convert ground-based measurement of transverse magnetic field power to equatorial plane azimuthal electric field power, a model-dependent transformation from the physical quantity measured.

Good overlap is seen in Figure 7 between results of the LFM-MIX simulations of both the 2013 (dashed purple) and 2015 (solid purple) storms and the D_{LL} coefficients obtained by *Ali et al.* [2016] based on in situ measurements of both electric and magnetic fields from Van Allen Probes. In all cases the vertical range in Figure 7 represents Kp variation. *Ali et al.* [2016] are limited to inside the apogee of Van Allen Probes (5.8 R_E) while the MHD simulations can be used to calculate radial diffusion coefficients at radial distances inside the magnetopause, which was outside of Van Allen Probes apogee for most of the 2015 and 2013 storms. Further, the MHD simulations covered times when Kp exceeded the $Kp = 5$ limit of the *Ali et al.* [2016] study, which was constrained by the requirement of acquiring an adequate statistical sample over all local times given the 19 month cadence of the Van Allen Probes orbit in magnetic local time (MLT) coverage. Both *Ali et al.* [2016] and *Ozeke et al.* [2014] studies are statistical studies from a large time interval. The diffusion coefficient during the two extreme events presented in this study shows a higher upper limit than average. Like prior measurement-based models, including *Brautigam and Albert* [2000] as well as *Ozeke et al.* [2014], *Ali et al.* [2016] assume that all power measured is occurring in the fundamental $m = 1$ mode. We are able to analyze the global mode structure in the MHD simulations, and power is summed over all m contributions below the Nyquist frequency of our simulation, 8.3 mHz, as described by *Li et al.* [2016]. Performing a subtraction analysis between results of our radial diffusion calculation and that measured by the MagEIS instrument on Van Allen Probes, we have found improved agreement using coefficients based on MHD simulation in the radial diffusion calculation relative to using *Brautigam and Albert* [2000] coefficients for the 17 March 2013 storm [*Li et al.*, 2014b]. We have incorporated the nonnegligible contribution of power at higher m numbers to the evaluation of diffusion coefficients. *Li et al.* [2016] showed that although $m = 1$, power is largest on 18 March 2015, used to calculate D_{LL} in this study, the contribution of $m = 2$ is ~50% and $m = 3$ is ~25% of $m = 1$, thus inclusion of higher m modes can be significant in evaluating the diffusion coefficients using equation (1). MHD specification of ULF wave power, which is required globally for calculating radial diffusion coefficients, and can only be known globally in a statistical sense from measurements, can be useful in deciding between data-based diffusion coefficients parameterized by Kp, not only in a 1-D radial diffusion model, but in 3-D models which have been developed [*Subbotin et al.*, 2011; *Tu et al.*, 2013]. Further analysis of ULF wave power level and mode structure in azimuthal electric field and compressional magnetic field components as a function of specified solar wind input [*Claudepierre et al.*, 2008, 2010] may lead to parametrizing D_{LL} by solar wind input rather than Kp, much as the Tsyganenko-Sitnov magnetic field model based on solar wind input has advanced, for example, over T89 specification by Kp of the global background magnetic field.

Acknowledgments

This work was supported by JHU/APL under NASA contracts NNN16AA09T and NNN06AA01C to UMN and UNH with subcontracts to Dartmouth. We would like to acknowledge high-performance computing support from Yellowstone provided by NCAR's Computational and Information Systems Laboratory, supported by the National Science Foundation. We thank David Malaspina for providing plasmapause location from EFW measurements of spacecraft potential for comparison with the Carpenter and Anderson model used in radial diffusion calculations shown. Van Allen Probe ECT data can be accessed at https://www.rbsp-ect.lanl.gov/rbsp_ect.php and EFW survey plots at http://rbsp.space.umn.edu/survey/.

References

Ali, A. F., D. M. Malaspina, S. R. Elkington, A. N. Jaynes, A. A. Chan, J. Wygant, and C. A. Kletzing (2016), Electric and magnetic radial diffusion coefficients using the Van Allen probes data, *J. Geophys. Res. Space Physics*, *121*, 9586–9607, doi:10.1002/2016JA023002.

Angelopoulos, V. (2009), *The THEMIS Mission*, Springer, New York.

Baker, D. N., et al. (2014), Gradual diffusion and punctuated phase space density enhancements of highly relativistic electrons: Van Allen Probes observations, *Geophys. Res. Lett.*, *41*, 1351–1358, doi:10.1002/2013GL058942.

Brautigam, D., and J. Albert (2000), Radial diffusion analysis of outer radiation belt electrons during the October 9, 1990, magnetic storm, *J. Geophys. Res.*, *105*(A1), 291–309, doi:10.1029/1999JA900344.

Brizard, A. J., and A. A. Chan (2001), Relativistic bounce-averaged quasilineaer diffusion equation for low-frequency electrmagnetic fluctuations, *Phys. Plasmas*, *8*, 4762–4771, doi:10.1063/1.1408623.

Blake, J. B., et al. (2013), The Magnetic Electron Ion Spectrometer (MagEIS) instruments aboard the Radiation Belt Storm Probes (RBSP) spacecraft, *Space Sci. Rev.*, *179*, 383–421, doi:10.1007/s11214-013-9991-8.

Carpenter, D., and R. Anderson (1992), An ISEE/Whistler model of equatorial electron density in the magnetosphere, *J. Geophys. Res.*, *97*(A2), 1097–1108, doi:10.1029/91JA01548.

Claudepierre, S., M. Hudson, W. Lotko, J. Lyon, and R. Denton (2010), Solar wind driving of magnetospheric ULF waves: Field line resonances driven by dynamic pressure fluctuations, *J. Geophys. Res.*, *115*, A11202, doi:10.1029/2010JA015399.

Claudepierre, S. G., S. R. Elkington, and M. Wiltberger (2008), Solar wind driving of magnetospheric ULF waves: Pulsations driven by velocity shear at the magnetopause, *J. Geophys. Res.*, *113*, A05218, doi:10.1029/2007JA012890.

Claudepierre, S. G., F. R. Toffoletto, and M. Wiltberger (2016), Global MHD modeling of resonant ULF waves: Simulation with and without a plasmasphere, *J. Geophys. Res. Space Physics*, *121*, 227–244, doi:10.1002/2015JA022048.

Cornwall, J. M. (1968), Diffusion processes influenced by conjugate-point wave phenomena, *Radio Sci.*, *3*, 740–744.

Elkington, S. R., M. K. Hudson, and A. A. Chan (2003), Resonant acceleration and diffusion of outer zone electrons in an asymmetric geomagnetic field, *J. Geophys. Res.*, *108*(A3), 1116, doi:10.1029/2001JA009202.

Elkington, S. R., A. A. Chan, and M. J. Wiltberger (2012), Global structure of ULF waves during the 24–26 September 1998 geomagnetic storm, in *Dynamics of the Earth's Radiation Belts and Inner Magnetosphere, Geographys. Monogr. Ser.*, edited by D. Summers et al., pp. 127–138, AGU, Washington, D. C., doi:10.1029/2012GM001348.

Fälthammar, C.-G. (1965), Effects of time-dependent electric fields on geomagnetically trapped radiation, *J. Geophys. Res.*, *70*(11), 2503–2516, doi:10.1029/JZ070i011p02503.

Fälthammar, C.-G. (1968), Radial diffusion by violation of the third adiabatic invariant, in *Earth's Particles and Fields, NATO Advanced Study Institute*, edited by B. M. McCormac, pp. 157–169, Van Nostrand Reinhold, New York.

Fei, Y., A. A. Chan, S. R. Elkington, and M. J. Wiltberger (2006), Radial diffusion and MHD particle simulations of relativistic electron transport by ULF waves in the September 1998 storm, *J. Geophys. Res.*, *111*, A12209, doi:10.1029/2005JA011211.

Fok, M.-C., N. Y. Buzulukova, S.-H. Chen, A. Glocer, T. Nagai, P. Valek, and J. D. Perez (2014), The comprehensive inner magnetosphere-ionosphere model, *J. Geophys. Res. Space Physics*, *119*, 7522–7540, doi:10.1002/2014JA020239.

Gabrielse, C., C. Harris, V. Angelopoulos, A. Artemyev, and A. Runov (2016), The role of localized inductive electric fields in electron injections around dipolarizing flux bundles, *J. Geophys. Res. Space Physics*, *121*, 9560–9585, doi:10.1002/2016JA023061.

Huang, C.-L., H. E. Spence, M. K. Hudson, and S. R. Elkington (2010), Modeling radiation belt radial diffusion in ULF wave fields: 2. Estimating rates of radial diffusion using combined MHD and particle codes, *J. Geophys. Res.*, *115*, A06216, doi:10.1029/2009JA014918.

Hudson, M., D. Baker, J. Goldstein, B. Kress, J. Paral, F. Toffoletto, and M. Wiltberger (2014), Simulated magnetopause losses and Van Allen Probe flux dropouts, *Geophys. Res. Lett.*, *41*, 1113–1118, doi:10.1002/2014GL059222.

Hudson, M., J. Paral, B. T. Kress, M. Wiltberger, D. N. Baker, J. C. Foster, D. L. Turner, and J. R. Wygant (2015), Modeling CME-shock driven storms in 2012–2013: MHD-test particle simulation, *J. Geophys. Res. Space Physics*, *120*, 1168–1181, doi:10.1002/2014JA020833.

Hudson, M. K., B. T. Kress, H.-R. Mueller, J. A. Zastrow, and J. B. Blake (2008), Relationship of the Van Allen radiation belts to solar wind drivers, *J. Atmos. Sol. Terr. Phys.*, *70*, 708–729, doi:10.1016/j.jastp.2007.11.003.

Hudson, M. K., T. Brito, S. Elkington, B. Kress, Z. Li, and M. Wiltberger (2012), Radiation belt 2D and 3D simulations for CIR-driven storms during Carrington Rotation 2068, *J. Atmos. Sol. Terr. Phys.*, *83*, 51–62, doi:10.1016/j.jastp.2012.03.017.

Jordanova, V. K., Y. Yu, J. T. Niehof, R. M. Skoug, G. D. Reeves, C. A. Kletzing, J. F. Fennell, and H. E. Spence (2014), Simulations of inner magnetosphere dynamics with an expanded RAM-SCB model and comparisons with Van Allen Probes observations, *Geophys. Res. Lett.*, *41*, 2687–2694, doi:10.1002/2014GL059533.

Kanekal, S. G., et al. (2016), Prompt acceleration of magnetospheric electrons to ultrarelativistic energies by the 17 March 2015 interplanetary shock, *J. Geophys. Res. Space Physics*, *121*, 7622–7635, doi:10.1002/2016JA022596.

Kim, H.-J., and A. A. Chan (1997), Fully adiabatic changes in storm time relativistic electron fluxes, *J. Geophys. Res.*, *102*(A10), 22,107–22,116.

Kress, B., M. Hudson, and J. Paral (2014), Rebuilding of the Earth's outer electron belt during 8–10 October 2012, *Geophys. Res. Lett.*, *41*, 749–754, doi:10.1002/2013GL058588.

Lanzerotti, L. J., and C. G. Morgan (1973), ULF geomagnetic power near $L = 4.2$. Temporal variation of radial diffusion-coefficient for relativistic electrons, *J. Geophys. Res.*, *78*(22), 4600–4610, doi:10.1029/JA078i022p04600.

Lanzerotti, L. J., D. C. Webb, and C. W. Arthur (1978), Geomagnetic field fluctuations at synchronous orbit, 2, Radial diffusion, *J. Geophys. Res.*, *83*, 3866–3870.

Le, G., et al. (2016), Magnetopause erosion during the 17 March 2015 magnetic storm: Combined field-aligned currents, auroral oval, and magnetopause observations, *Geophys. Res. Lett.*, *43*, 2396–2404, doi:10.1002/2016GL068257.

Li, W., et al. (2014), Radiation belt electron acceleration by chorus waves during the 17 March 2013 storm, *J. Geophys. Res. Space Physics*, *119*, 4681–4693, doi:10.1002/2014JA019945.

Li, Z., M. Hudson, and Y. Chen (2014a), Radial diffusion comparing a THEMIS statistical model with geosynchronous measurements as input, *J. Geophys. Res. Space Physics*, *119*, 1863–1873, doi:10.1002/2013JA019320.

Li, Z., M. K. Hudson, A. N. Jaynes, A. J. Boyd, D. M. Malaspina, S. A. Thaller, J. R. Wygant, and M. G. Henderson (2014b), Modeling gradual diffusion changes in radiation belt electron phase space density for the March 2013 Van Allen Probes case study, *J. Geophys. Res. Space Physics*, *119*, 8396–8403, doi:10.1002/2014JA020359.

Li, Z., M. Hudson, B. T. Kress, and J. Paral (2015), Three-dimensional test particle simulation of the 17–18 March 2013 CME shock-driven storm, *Geophys. Res. Lett.*, *42*, 5679–5685, doi:10.1002/2015GL064627.

Li, Z., M. Hudson, J. Paral, M. Wiltberger, and D. Turner (2016), Global ULF wave analysis of radial diffusion coefficients using a global MHD model for the 17 March 2015 storm, *J. Geophys. Res. Space Physics*, *121*, 6196–6206, doi:10.1002/2016JA022508.

Liu, W., W. Tu, X. Li, T. Sarris, Y. Khotyaintsev, H. Fu, H. Zhang, and Q. Shi (2016), On the calculation of electric diffusion coefficient of radiation belt electrons with in situ electric field measurements by THEMIS, *Geophys. Res. Lett.*, *43*, 1023–1030, doi:10.1002/2015GL067398.

Lyon, J., J. Fedder, and C. Mobarry (2004), The Lyon–Fedder–Mobarry (LFM) global MHD magnetospheric simulation code, *J. Atmos. Sol. Terr. Phys.*, *66*(15), 1333–1350, doi:10.1016/j.jastp.2004.03.020.

Mauk, B., N. J. Fox, S. Kanekal, R. Kessel, D. Sibeck, and A. Ukhorskiy (2013), Science objectives and rationale for the radiation belt storm probes mission, *Space Sci. Rev.*, *179*, 3–27, doi:10.1007/s11214-012-9908-y.

Merkin, V., and J. Lyon (2010), Effects of the low-latitude ionospheric boundary condition on the global magnetosphere, *J. Geophys. Res.*, *115*, A10202, doi:10.1029/2010JA015461.

Orlova, K., and Y. Shprits (2014), Model of lifetimes of the outer radiation belt electrons in a realistic magnetic field using realistic chorus wave parameters, *J. Geophys. Res. Space Physics*, *119*, 770–780, doi:10.1002/2013JA019596.

Orlova, K., M. Spasojevic, and Y. Shprits (2014), Activity dependent global model of electron loss inside the plasmasphere, *Geophys. Res. Lett.*, *41*, 3744–3751, doi:10.1002/2014GL060100.

Ozeke, L. G., and I. R. Mann (2004), Modeling the properties of guided poloidal Alfvén waves with finite asymmetric ionospheric conductivities in a dipole field, *J. Geophys. Res.*, *109*, A05205, doi:10.1029/2003JA010151.

Ozeke, L. G., I. R. Mann, K. R. Murphy, I. Jonathan Rae, and D. K. Milling (2014), Analytic expressions for ULF wave radiation belt radial diffusion coefficients, *J. Geophys. Res. Space Physics*, *119*, 1587–1605, doi:10.1002/2013JA019204.

Pembroke, A., F. Toffoletto, S. Sazykin, M. Wiltberger, J. Lyon, V. Merkin, and P. Schmitt (2012), Initial results from a dynamic coupled magnetosphere-ionosphere-ring current model, *J. Geophys. Res.*, *117*, A02211, doi:10.1029/2011JA016979.

Perry, K., M. Hudson, and S. Elkington (2005), Incorporating spectral characteristics of Pc5 waves into three-dimensional radiation belt modeling and the diffusion of relativistic electrons, *J. Geophys. Res.*, *110*, A03215, doi:10.1029/2004JA010760.

Reeves, G. D., et al. (2013), Electron acceleration in the heart of the Van Allen radiation belts, *Science*, *341*, 991–994, doi:10.1126/science.1237743.

Roederer, J. G. (1970), *Dynamics of Geomagnetically Trapped Radiation, Phys. and Chem. in Space*, vol. 2, Springer, Berlin.

Shprits, Y. Y., R. M. Thorne, R. Friedel, G. D. Reeves, J. Fennell, D. N. Baker, and S. G. Kanekal (2006), Outward radial diffusion driven by losses at magnetopause, *J. Geophys. Res.*, *111*, A11214, doi:10.1029/2006JA011657.

Shprits, Y. Y., S. R. Elkington, N. P. Meredith, and D. A. Subbotin (2008a), Review of modeling of losses and sources of relativistic electrons in the outer radiation belt I: Radial transport, *J. Atmos. Sol. Terr. Phys.*, *70*(14), 1679–1693, doi:10.1016/j.jastp.2008.06.008.

Shprits, Y. Y., D. A. Subbotin, N. P. Meredith, and S. R. Elkington (2008b), Review of modeling of losses and sources of relativistic electrons in the outer radiation belt II: Local acceleration and loss, *J. Atmos. Sol. Terr. Phys.*, *70*(14), 1694–1713, doi:10.1016/j.jastp.2008.06.014.

Spence, H. E., et al. (2014), Science goals and overview of the Energetic Particle, Composition, and Thermal Plasma (ECT) Suite on NASA's Radiation Belt Storm Probes (RBSP) mission, *Space Sci. Rev.*, *179*, 311–336, doi:10.1007/s11214-013-0007-5.

Southwood, D. J., and M. G. Kivelson (1981), Charged particle behavior in low-frequency geomagnetic pulsations 1. Transverse waves, *J. Geophys. Res.*, *86*, 5643–5655, doi:10.1029/JA086iA07p05643.

Subbotin, D. A., Y. Y. Shprits, and B. Ni (2011), Long-term radiation belt simulation with the VERB 3-D code: Comparison with CRRES observations, *J. Geophys. Res.*, *116*, A12210, doi:10.1029/2011JA017019.

Thorne, R. M. (2010), Radiation belt dynamics: The importance of wave-particle interactions, *Geophys. Res. Lett.*, *37*, L22107, doi:10.1029/2010GL044990.

Tsurutani, B. T., and W. D. Gonzalez (1997), The interplanetary causes of magnetic storms: A review, in *Magnetic Storms, Geophys. Monogr. Ser.*, edited by B. T. Tsurutani et al., pp. 77–89, AGU, Washington, D. C.

Tsurutani, B. T., et al. (2006), Corotating solar wind streams and recurrent geomagnetic activity: A review, *J. Geophys. Res.*, *111*, A07S01, doi:10.1029/2005JA011273.

Tu, W., S. R. Elkington, X. Li, W. Liu, and J. Bonnell (2012), Quantifying radial diffusion coefficients of radiation belt electrons based on global MHD simulation and spacecraft measurements, *J. Geophys. Res.*, *117*, A10210, doi:10.1029/2012JA017901.

Tu, W., G. Cunningham, Y. Chen, M. Henderson, E. Camporeale, and G. Reeves (2013), Modeling radiation belt electron dynamics during GEM challenge intervals with the dream3d diffusion model, *J. Geophys. Res. Space Physics*, *118*, 6197–6211, doi:10.1002/jgra.50560.

Vampola, A. L. (1996), The ESA outer zone electron model update, in *Environment Modeling for Spaced-Based Applications, Space Sci. Rev.*, edited by W. Burke and T.-D. Guyenne, pp. 151–158, ESTEC, Noordwijk, Netherlands.

Wygant, J., et al. (2014), The electric field and waves instruments on the radiation belt storm probes mission, *Space Sci. Rev.*, *179*, 183–220, doi:10.1007/s11214-013-0013-7.